CHEMICAL AND CRYSTALLOGRAPHIC CHARACTERISATION OF A GROSSMANITE-BEARING CALCIUM-ALUMINIUM-RICH INCLUSION WITHIN THE WINCHCOMBE CM2 CARBONACEOUS CHONDRITE. P-E. M. C. Martin[1], A. J. King[2], J. Spratt[2], L. Daly[1,3,4], and M. R. Lee[1], [1]School of Geographical and Earth Sciences, University of Glasgow, Glasgow, UK. [2]Natural History Museum, London, UK. [3]Australian Centre for Microscopy and Microanalysis, The University of Sydney, Sydney, NSW, Australia. [4]Department of Materials, University of Oxford, Oxford, UK. (p.martin.2@research.gla.ac.uk).

Introduction: Despite being amongst the most common carbonaceous meteorite samples, many questions remain as to the origin and evolution of the CM parent body(-ies). As refractory inclusions are the first solids to have formed in the solar system, studying them is crucial in perfecting our understanding of it.

Winchcombe is a veritable cornucopia of carbonaceous lithologies and the perfect candidate for studying refractory objects such as Calcium-Aluminium-rich Inclusions (CAIs) within the CM (Mighei-like) carbonaceous group. The meteorite is composed of eight main lithologies displaying varying degrees of aqueous alteration, ranging from CM2.0 to 2.6 (**[1]**), according to the classification of **[2, 3]**.

All CAIs within the meteorite have a core containing spinel, perovskite, or an assemblage of both, alongside olivine and/or pyroxene **[4]**. However, unusually Ti-rich pyroxenes have been identified within a CAI located in lithology A (CM2.2, **[1]**) of Winchcombe. Here, we report the occurrence, petrographic and crystallographic properties, and composition of grossmanite, $Ca(Ti^{3+},Mg,Ti^{4+})AlSiO_6$, a Ti-rich clinopyroxene **[5]**, within the Winchcombe meteorite. This distinctive mineral has the potential to provide insights into the origins of Winchcombe's constituents.

Materials and Methods: The CAI was identified within polished block P30552 using sample-wide Backscattered Electron (BSE) images combined with Ca-Al-Mg Energy-Dispersive X-ray Spectroscopy (EDS) maps produced by Scanning Electron Microscopy (SEM) at the Natural History Museum (NHM), London (20 kV/3 nA, live frame time 270s). The block was then further studied to confirm the mineralogy of the CAI using a Zeiss Sigma Variable Pressure Analytical SEM (20 kV/1-2 nA) at the University of Glasgow (UoG).

Crystallographic characterisation was also carried out at the UoG by Transmission Electron Microscopy (TEM) alongside Transmission Kikuchi Diffraction (TKD), the latter using a Zeiss Sigma Variable Pressure Analytical SEM (20 kV/1-2 nA) equipped with an NordlysMax2 Electron Backscatter Diffraction (EBSD) detector using a 0.02 µm step size. All crystallographic data were collected using the Aztec v5.1 software and processed using AZtec Crystal v2.1 from Oxford Instruments.

Grossmanite grains (~1 µm in size) and other phases (i.e. spinel, perovskite) within the CAI were further characterised using the JEOL JXA-8530F Electron Microprobe (10 kV/20 nA; EPMA) in a focused beam mode at the NHM. The detection limits have been estimated at ~100 ppm (SD × 3). **Table 1** displays the average of eight individual analyses from eight grossmanite grains.

Results: The dimensions of the CAI are 138 × 206 µm in the section plane and it is surrounded by a quasi-complete ~10 µm-thick Fine-Grained Rim (FGR; circled within the blue dashed line in **Fig. 1**), itself surrounded by patches of Tochilinite-Cronstedtite Intergrowths (TCIs; bright patches in BSE in **Fig. 1**) within the matrix.

	wt%	Range		SD
		min.	max.	
SiO_2	28.61	25.84	29.89	1.38
Al_2O_3	22.96	21.92	23.76	0.61
CaO	25.22	24.56	26.36	0.61
TiO_2*	15.90	14.34	18.64	1.27
MgO	4.87	4.23	5.42	0.42
V_2O_5	1.10	0.74	1.46	0.28
FeO	0.22	0.05	0.46	0.11
Cr_2O_3	0.17	<dt	0.25	0.08
NiO	0.15	<dt	0.18	0.02
Na_2O	0.07	<dt	0.07	<dt
Total	99.28			

Table 1. *Average composition (n = 8) of grossmanite grains obtained by EPMA. TiO_2* corresponds to total titanium (no differentiation between Ti^{3+} and Ti^{4+}). Only measurements with 97-101 wt% totals were considered.*

The CAI is heavily calcitised and is mainly composed of calcite ($CaCO_3$; cf. **Fig. 1a**), with a rim structure (appearing as a lighter area of a higher atomic number in BSE; cf. **Fig. 1a**) comprising a few sparse globular micrometric (~10 µm) grains of spinel ($MgAl_2O_4$; cf. **Fig. 1a**) spread alongside its inner edges. A core region set on one side of the CAI is composed of sparse micrometric clusters of small (1-5 µm) grains of

perovskite ($CaTiO_3$; cf. **Fig. 1b**) and oblong grossmanite (cf. **Fig. 1b**). The rim structure within the calcite host is very well defined within the Inverse Pole Figure TKD map (IPF, cf. **Fig. 2**) and comprises two adjacent calcite sub-grains with different crystallographic orientations (cf. **Fig. 2**).

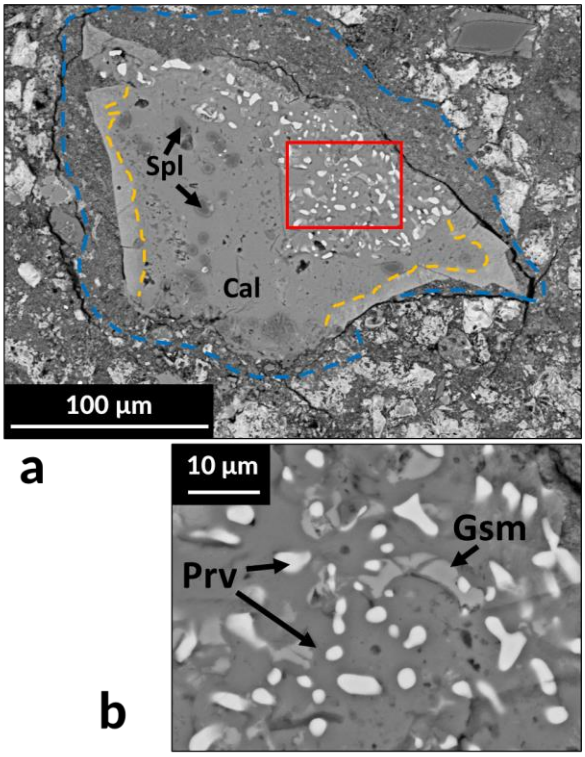

Fig. 1. (**a**) *BSE image of the grossmanite-bearing CAI in Winchcombe. Globular dark spinel (Spl) grains are within the calcite (Cal) portion of the inclusion. The yellow dashed line indicates the boundary between the inner calcite and the calcite rim. The dashed blue line shows the outer edge of the FGR enclosing the CAI.* (**b**) *Enlarged BSE image (area marked in red) showing grossmanite (Gsm) and perovskite (Prv) grains within a Cal host. Figures modified from* **[7]**.

Due to its irregular shape, and the nature and variance of the textures of different areas within the CAI, it is considered a complex aggregate for the purposes of the CAI classification established by **[6]**.

Discussion: A grossmanite-bearing CAI was described from the Allende meteorite (CV3) by **[5]** where the Ti-rich pyroxene is inferred to have formed after spinel and perovskite but before the crystallisation of melilite. This paragenesis agrees with our observations as the spinel grains appear to be globular and larger than the rest of the refractory phases within the CAI. EBSD data, through Grain Reference Orientation Deviation (GROD) angle maps, show minimal deviation of internal grain orientation indicating that the calcite, grossmanite, and the perovskite are relatively undeformed within the core region of the CAI. This texture, in addition to their boundaries being well defined, suggests a slow and unperturbed crystallisation. Furthermore, the boundary between both Cal 1 (green in **Fig. 2**) and Cal 2 (dark blue in **Fig. 2**) could have stemmed from the replacement of anorthite (or even melilite **[8, 9]**), with Cal 2 forming the rim as it envelops the entire CAI under the surface of the section (cf. **Fig. 2**).

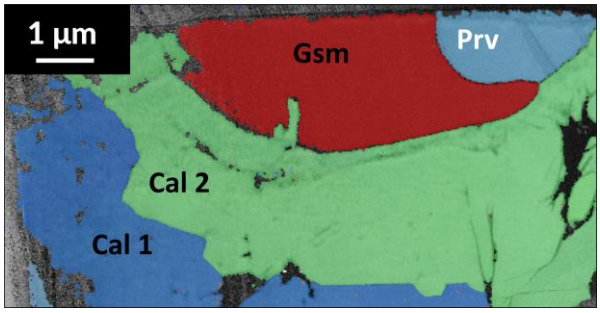

Fig. 2. *Inverse Pole Figure |Z| (IPF) map of a FIB (Focused Ion Beam) slice of the investigated CAI produced for TKD. The image shows differences in crystallographic orientations of the grains. The grossmanite grain (Gsm) appears to partially cover the perovskite (Prv), which could suggest that it formed later (or potentially simultaneously from two immiscible fluids). The contact between the two calcite sub-grains (Cal 1 and Cal 2) is sharp. Twinning can be observed in the Prv (light gray stripe in the top right corner of the image) but is only visible in the band contrast map as it wasn't resolved by the Kikuchi pattern.*

Studying the petrology of such uncommon occurrences within the CAI populations can provide invaluable insight on the evolution and origin of the CM parent body(-ies), and thus on the formation of the Solar System. Future work will investigate the twinning in the perovskite using TKD to constrain its thermal history **[10]** and refine our understanding of the formation of grossmanite-bearing CAIs within carbonaceous meteorites.

References: [1] Suttle M. D. et al. (2022) *M&PS*, 1–25. **[2]** Rubin A. et al. (2007) *GCA*, 71 (9), 2361–2382. **[3]** Rubin A. (2015) *M&PS*, 50 (9), 1595–1612. **[4]** Martin P-E. M. C. et al. (in prep.). **[5]** Ma C. & Rossman G. R. (2009) *Am. Min.*, 94, 1491–1494. **[6]** MacPherson G. R. & Davis A. M. (1994) *GCA*, 58 (24), 5599–5625. **[7]** Martin P-E. M. C. et al. (2022) *85th Met. Soc.*, 6358. **[8]** Stolper E. (1982) *GCA*, 46, 2159–2180. **[9]** Hewins R. H. et al. (2005) *ASP* 341 286–316. **[10]** Keller L. P. & Busek P. R. (1994) *Am. Min.*, 79, 73–79.